
ENHANCING SPATIO-TEMPORAL FORECASTING WITH SPATIAL NEIGHBOURHOOD FUSION: A CASE STUDY ON COVID-19 MOBILITY IN PERU

Chuan Li* Jiang You† Hassine Moun gla‡ Vincent Gauthier§ Miguel Nunez-del-Prado¶

Hugo Alatr ista-Salas||

July 2, 2025

ABSTRACT

Accurate modeling of human mobility is critical for understanding epidemic spread and deploying timely interventions. In this work, we leverage a large-scale spatio-temporal dataset collected from Peru’s national Digital Contact Tracing (DCT) application during the COVID-19 pandemic to forecast mobility flows across urban regions. A key challenge lies in the spatial sparsity of hourly mobility counts across hexagonal grid cells, which limits the predictive power of conventional time series models. To address this, we propose a lightweight and model-agnostic *Spatial Neighbourhood Fusion* (SPN) technique that augments each cell’s features with aggregated signals from its immediate H3 neighbors. We evaluate this strategy on three forecasting backbones—NLinear, PatchTST, and K-U-Net—under various historical input lengths. Experimental results show that SPN consistently improves forecasting performance, achieving up to 9.85% reduction in test MSE. Our findings demonstrate that spatial smoothing of sparse mobility signals provides a simple yet effective path toward robust spatio-temporal forecasting during public health crises.

1 Introduction

Human mobility is one of the strongest macroscopic drivers of infectious-disease dynamics. During the COVID-19 pandemic, aggregated mobile-phone traces provided unprecedented visibility into how non-pharmaceutical interventions (NPIs) reshaped population movement and, in turn, epidemic curves [1, 2]. Digital contact-tracing (DCT) platforms push this visibility to an even finer scale, recording person-to-person proximity events in near real time. Peru was an early adopter: its Perú en tus manos app merged Bluetooth encounters with DCT positioning and has remained one of the few fully operational national DCT systems in Latin America [3]. The resulting data stream, covering millions of users, opens a unique opportunity to model urban mobility flows in settings where official traffic sensors or ticketing logs are scarce.

Yet transforming raw proximity pings into reliable origin–destination (OD) counts is non-trivial. Spatial discretisation with hexagonal H3 cells offers a principled way to regularise geometry and enable efficient spatial joins [4]. At the hourly resolution required for real-time public-health response, however, most cells contain few or zero trips, leading to extreme sparsity [5]. While deep spatio-temporal models—ranging from graph neural networks to Transformer

*LIPADE, Université Paris Cité; EDITE, Sorbonne Université; Telecom SudParis; Institut Polytechnique de Paris. chuan.li@sorbonne-universite.fr

†LISSI, Université Paris-Est Créteil; ESIEE Paris (UGE). jiang.you@esiee.fr

‡LIPADE, Université Paris Cité; Telecom SudParis; Institut Polytechnique de Paris. hassine.moungla@parisdescartes.fr

§SAMOVAR, Telecom SudParis; Institut Polytechnique de Paris. vincent.gauthier@telecom-sudparis.eu

¶The World Bank, Washington DC, USA. mnunezdelpradoco@worldbank.org

||Léonard de Vinci Pôle Universitaire – Research Center, Paris, France. hugo.alatr ista_salas@devinci.fr

variants—can learn complex dependencies, they often overfit noisy zero-inflated inputs or fail to extrapolate when data gaps appear [6, 7].

We address this challenge with a lightweight Spatial Neighbourhood Fusion (SPN) scheme that augments each H3 cell’s signal with robust statistics from its immediate neighbours. SPN acts as a plug-and-play preprocessing layer and can be paired with any forecasting backbone. Using a large-scale dataset from Peru’s national DCT deployment, we show that SPN consistently reduces test-set MSE across three representative models (NLinear, PatchTST, K-U-Net) and four input horizons, highlighting the value of local spatial smoothing for epidemic-era mobility prediction.

2 Related Work

2.1 Mobility Data for Epidemic Intelligence

Early COVID-19 studies established that decreases in inter-provincial travel preceded lower case growth in multiple regions. Oliver et al. synthesised best practices for using telecom data throughout the pandemic life-cycle, emphasising privacy safeguards and representativeness [1]. Parallel work coupled mobility networks with compartmental models or gravity kernels to explain city-level reproduction numbers [8].

2.2 Digital Contact Tracing Datasets

Beyond aggregated tower pings, DCT platforms offer metre-level resolution of interpersonal encounters. Serafino et al. demonstrated that billions of GPS-level contacts capture the changing topology of transmission networks and can inform targeted quarantine policies [9]. Peru’s Perú en tus manos remains a flagship example of nationwide deployment, providing anonymised GPS + Bluetooth traces that have been used for both epidemiological analysis and mobility research [3].

2.3 Spatio-Temporal Forecasting Models

Graph-based deep learners such as HiSTGNN [6] and ST-GNN variants [10] fuse spatial adjacency with temporal convolutions to predict case counts or traffic volumes, but require dense observations at every node. Transformer architectures have been adapted to long-horizon time-series tasks; PatchTST segments inputs into patches to alleviate quadratic attention costs and currently leads many public benchmarks [7]. Conversely, the NLinear family of embarrassingly simple linear nets questions whether heavy architectures are needed at all [11]. All these models, however, are sensitive to the zero-inflation that arises when fine-grid mobility is sparsely sampled.

2.4 Spatial Smoothing and Data Augmentation

Neighbourhood aggregation is a classical remedy for sparse geospatial counts, from remote-sensing gap-filling [12] to adaptive traffic forecasting [13]. Median-based fusion, in particular, is robust to outliers and has low computational overhead—properties that motivate our SPN design.

Positioning of this work. Where prior studies rely on complex graph diffusion or attention layers to propagate information, we show that a model-agnostic, first-order neighbourhood median is sufficient to boost performance on a real, country-scale DCT dataset. SPN thus complements, rather than competes with, existing deep architectures and can be deployed at almost no extra cost, a feature that is crucial for low-resource public-health settings.

3 Data Pre-processing

We analyse GPS traces collected by Peru’s national Digital Contact Tracing (DCT) application between April and June 2020. The raw dataset contains 808 M location pings from 1.58 M users. Restricting the sample to “active” users—those with at least 30 pings—yields 651 k reliable trajectories. Descriptive statistics appear in Table 1. Pre-processing by Algorithm 1.

Algorithm 1 Pre-processing pipeline for DCT mobility data**Require:** Raw tuples $(u, t, \varphi, \lambda, status)$ **Ensure:** Hourly OD tensor OD, inflow IN, outflow OUT

```

1: User filtering
2:  $A \leftarrow \{\text{users with } \geq 30 \text{ pings}\}$ 
3:  $\mathcal{R} \leftarrow \text{records with } u \in A \text{ and time } \in \text{Apr.} \text{--} \text{Jun. 2020}$ 
4: Stop-point extraction (per user)
5: for trajectory of user  $u \in A$  do
6:   initialise cluster  $\mathcal{C} \leftarrow \emptyset$ 
7:   for point  $p$  in time order do
8:     if  $\text{dist}(p, \text{medoid}(\mathcal{C})) \leq 50\text{m}$  and  $\text{elapsed} \leq 5 \text{ min}$  then
9:        $\mathcal{C} \leftarrow \mathcal{C} \cup \{p\}$ 
10:    else
11:      if  $\text{duration}(\mathcal{C}) \geq 5 \text{ min}$  then
12:        emit stop  $\sigma_u \leftarrow \text{medoid}(\mathcal{C})$ 
13:      end if
14:       $\mathcal{C} \leftarrow \{p\}$  {start new cluster}
15:    end if
16:  end for
17: end for
18:  $\mathcal{S} \leftarrow \text{all emitted stops}$ 
19: Spatial discretisation
20: for stop  $\sigma \in \mathcal{S}$  do
21:    $\sigma.h3 \leftarrow \text{GEOToH3}(\sigma.\varphi, \sigma.\lambda, \text{res} = 6)$ 
22: end for
23: OD counting
24: initialise OD  $[d, h, s, t] \leftarrow 0$ 
25: for user  $u \in A$  do
26:   for consecutive stops  $(\sigma_k, \sigma_{k+1})$  do
27:      $(d, h) \leftarrow \text{date+hour of } \sigma_k$ 
28:      $\text{OD}[d, h, \sigma_k.h3, \sigma_{k+1}.h3] += 1$ 
29:   end for
30: end for
31: In/Out aggregation
32: for all  $d, h, c$  do
33:    $\text{IN}[d, h, c] \leftarrow \sum_s \text{OD}[d, h, s, c]$ 
34:    $\text{OUT}[d, h, c] \leftarrow \sum_t \text{OD}[d, h, c, t]$ 
35: end for
36: return OD, IN, OUT

```

Table 1: Dataset overview

Records with DCT fix	808,021,726
Users with DCT records	1,581,867
Active users (≥ 30 records)	651,155
App downloads (census)	1,896,228
Study period	Apr.–Jun. 2020
Cumulative infected users	81,305
Infected users with DCT data	10,131

3.1 Spatial Neighbourhood Feature Fusion (SPN)

Due to the sparsity of mobility signals in certain H3 cells at specific timestamps, we propose a lightweight yet effective technique named **Spatial Neighbourhood Fusion (SPN)** to enhance temporal continuity through local spatial aggregation.

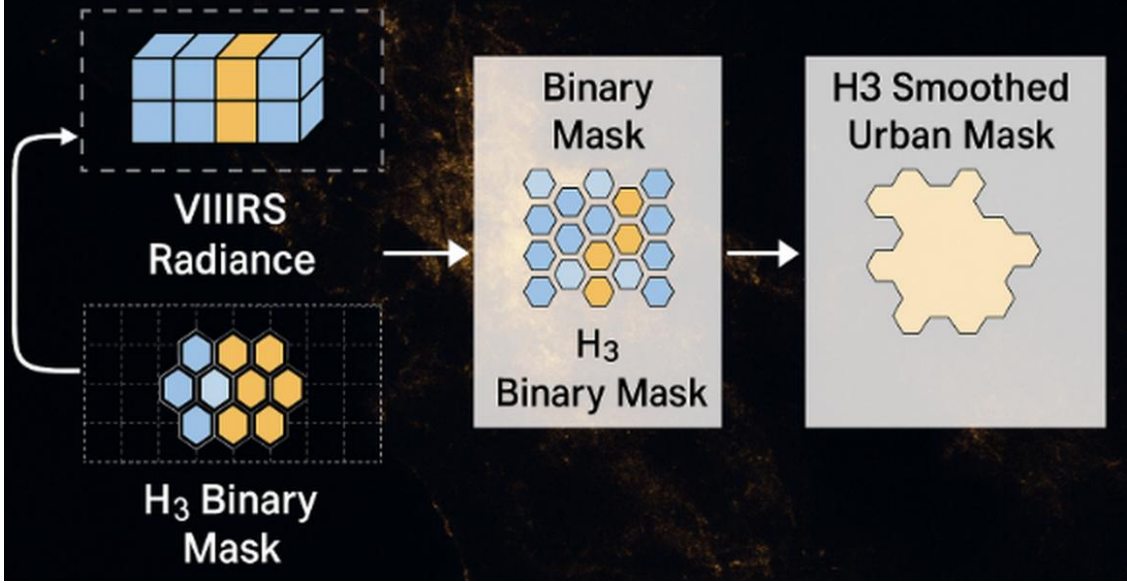


Figure 1: Urban mask construction guided by night-time lights. Raw VIIRS radiance is first aligned with the H3 grid system, yielding a binary mask where cells above the radiance threshold ($8 \text{ nW cm}^{-2} \text{ sr}^{-1}$) are marked as urban. This binary urban mask is then smoothed using kernel density estimation to form contiguous urban clusters. The resulting H3-smoothed mask enables downstream models to differentiate between urban and peri-urban dynamics.

Given a hexagonal cell c at time t , we define its estimated spatial flow as the median of non-zero total flows among its immediate neighbors:

$$\hat{f}_c^{(t)} = \text{median} \left\{ f_n^{(t)} \mid n \in \mathcal{N}(c), f_n^{(t)} > 0 \right\}, \quad (1)$$

where $f_n^{(t)}$ denotes the observed total flow in cell n at time t , and $\mathcal{N}(c) = \text{grid_disk}(c, 1) \setminus \{c\}$ is the first-order spatial neighborhood defined by the H3 indexing system.

If no valid neighbors exist (i.e., all neighbors are missing or zero-valued), we fallback to the cell’s original value: $\hat{f}_c^{(t)} \leftarrow f_c^{(t)}$.

To further stabilize the signal, we compute the arithmetic mean of the original and spatially aggregated flow:

$$\bar{f}_c^{(t)} = \frac{1}{2} \left(f_c^{(t)} + \hat{f}_c^{(t)} \right). \quad (2)$$

Finally, we construct a three-channel feature vector for each cell and time step as:

$$\mathbf{x}_c^{(t)} = \left[f_c^{(t)}, \hat{f}_c^{(t)}, \bar{f}_c^{(t)} \right].$$

This SPN operation is non-parametric, model-agnostic, and computationally efficient (under 4 ms per hourly snapshot on standard hardware).

3.2 Night-lights-guided Urban Mask

To distinguish urban from peri-urban H3 cells, we leverage radiance data from the Visible Infrared Imaging Radiometer Suite (VIIRS) [14]. Empirical studies show that urban cores typically exceed $10 \text{ nW cm}^{-2} \text{ sr}^{-1}$ [15], where the unit $\text{nW cm}^{-2} \text{ sr}^{-1}$ denotes nanowatts of radiative power per square centimeter per steradian—a standard measure of optical radiance. We adopt a conservative threshold of $8 \text{ nW cm}^{-2} \text{ sr}^{-1}$, then smooth the resulting binary mask using kernel density estimation to form contiguous urban clusters [16]. Temporal stacks of VIIRS images allow us to track urban growth over the study window [17], providing an external validity check for the SPN-enhanced mobility flows.

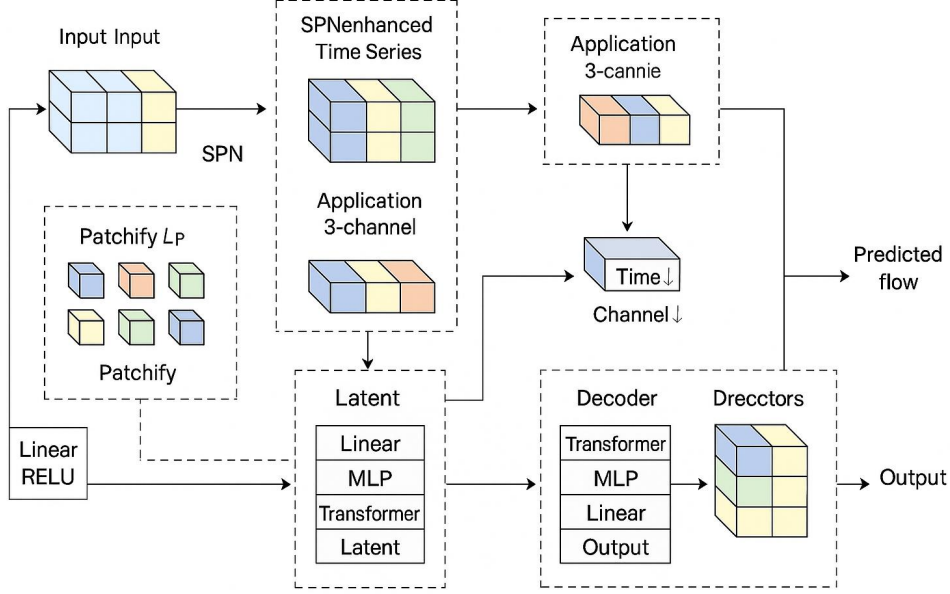


Figure 2: End-to-end forecasting pipeline. An **SPN** block (left, not shown) fuses each H3 cell with the median of its six neighbours; the resulting three-channel tensor ($L \times 3$) is patch-embedded and fed into one of three backbones. *NLinear* applies channel-wise linear layers; *PatchTST* operates on non-overlapping patches with a Transformer encoder; *Kernel U-Net* (centre) uses a symmetric encoder–decoder whose blocks wrap custom kernels (Linear, MLP, LSTM, Transformer). Skip connections preserve high-resolution context, and the latent vector is jointly down-sampled along time and channel dimensions. All backbones output the predicted mobility flow for the next T hours.

4 Method

4.1 Problem formulation

Let $\mathbf{x} \in \mathbb{R}^{N \times M}$ be the multivariate time series containing N time steps (hours) and M features (H3 cells). For a look-back window of length L and a forecasting horizon T , the task is

$$(\hat{\mathbf{x}}_{t+1}, \dots, \hat{\mathbf{x}}_{t+T}) = f_{\theta}(\mathbf{x}_{t-L+1}, \dots, \mathbf{x}_t), \quad t \in [L, N - T],$$

where f_{θ} denotes a learnable mapping.

SPN-enhanced input. Prior to modelling we apply Spatial Neighbourhood Fusion (SPN): for each cell c and hour t we compute the neighbourhood median $\hat{f}_c^{(t)}$ and the mean $\bar{f}_c^{(t)} = \frac{1}{2}(f_c^{(t)} + \hat{f}_c^{(t)})$ of the original flow $f_c^{(t)}$. The model therefore ingests a three-channel tensor $[f_c^{(t)}, \hat{f}_c^{(t)}, \bar{f}_c^{(t)}]$.

4.2 Backbone library

- **NLinear** [11]: a stack of channel-wise linear layers; parameter-efficient baseline.
- **PatchTST** [7]: partitions the series into patches of length $L_p=4$ and feeds them to a Transformer encoder, achieving $O(L/L_p)$ complexity.
- **Kernel U-Net (K-U-Net)** [18]: a symmetric encoder–decoder whose blocks wrap custom kernels. We use a Linear→MLP→Transformer hierarchy in the encoder and its mirror in the decoder; skip connections preserve high-resolution context (see Fig. 2).

+spn variants. For each backbone we train a vanilla one-channel model and an SPN-enhanced three-channel counterpart, denoted *NLinear+spn*, *PatchTST+spn*, and *K-U-Net+spn*. Apart from the input dimension, all hyper-parameters remain unchanged, isolating the gain from spatial fusion.

Table 2: Multivariate time-series forecasting on the *smoothed* mobility-flow dataset. Look-back $L \in \{48, 72, 96, 120\}$; horizon $T = 48$. Lower MSE is better. Best scores are **bold**; second best are underlined. ‘‘Avg Imp.’’ reports the % improvement of each ‘‘+ spn’’ variant over its backbone.

Method	L	Linear		Linear+spn		PatchTST		PatchTST+spn		K-U-Net		K-U-Net+spn	
		Train	Test	Train	Test	Train	Test	Train	Test	Train	Test	Train	Test
Length	48	0.4343	0.4146	0.4033	0.3834	0.4097	0.3848	0.3753	<u>0.3675</u>	0.3553	0.3838	0.3173	0.3535
	72	0.4160	0.3959	0.3828	0.3615	0.3993	0.3780	0.3589	<u>0.3493</u>	0.3155	0.3758	0.3002	0.3459
	96	0.4138	0.3902	0.3798	0.3539	0.3950	0.3818	0.3565	<u>0.3481</u>	0.2963	0.3745	0.2718	0.3462
	120	0.4173	0.4098	0.3829	<u>0.3742</u>	0.3951	0.3826	0.3528	<u>0.3999</u>	0.3218	0.3937	0.2717	0.3472
Avg Imp. (%)		—	—	7.89	8.55	—	—	9.75	8.00	—	—	9.85	8.80

4.3 Dataset

After filtering (Sec. III) the mobility cube contains $N = 577$ hourly steps and $M = 101$ H3 cells. We adopt a chronological split of 70%/10%/20% for training, validation, and testing.

5 Experiments and Results

5.1 Experimental settings

Because public-health planners are interested in trends rather than momentary peaks, we follow the pipeline in Fig. 2 and predict the SPN-smoothed flow series. For each H3 cell we form $flow_clean_t = \alpha flow_total_t + (1 - \alpha) median_t$, where the tilde denotes the median of its six neighbours and $\alpha = 0.5$ is chosen on the validation split (grid-search $\alpha \in \{1.0, 0.9, \dots, 0.0\}$).

Six models—*NLinear*, *NLinear+spn*, *PatchTST*, *PatchTST+spn*, *K-U-Net*, and *K-U-Net+spn*—are benchmarked on look-back windows $L \in \{48, 72, 96, 120\}$ with a forecasting horizon of $T = 48$ h. Each ‘‘+spn’’ variant receives an extra channel that contains the lag-1 neighbour-median; its backbone only sees the lag-1 self-history.

Optimisation. All runs minimise MSE with the Adam optimiser ($lr = 5 \times 10^{-4}$), batch size 128, and early stopping on a 10 % validation split (patience 50). PatchTST and K-U-Net use a hidden size of 128; K-U-Net width factors are $\langle 6, 2 \rangle$, $\langle 6, 3 \rangle$, $\langle 6, 4 \rangle$, $\langle 6, 5 \rangle$ for $L = 48, 72, 96, 120$, respectively. Each configuration is repeated with five random seeds and we report the mean and—where space permits—its standard deviation.

5.2 Main results

Table 2 lists train- and test-set MSE (lower is better) on the smoothed target. Across all three backbones, adding SPN features **consistently reduces error**.

- **NLinear+spn** lowers test MSE by an average **8.6 %** (7.9 % on the train split).
- **PatchTST+spn** achieves a mean **8.0 %** test-set gain, with the largest relative drop (9.75 %) on the train split at $L=96$.
- **K-U-Net+spn** gives the strongest improvement: a mean **8.8 %** reduction in test MSE and up to 0.030 absolute gain on the $L=72$ configuration.

Improvements are most pronounced for the shorter windows ($L=48$ and 72), supporting our hypothesis that neighbourhood fusion is particularly helpful when the temporal context is limited.

6 Conclusion

Leveraging nationwide mobility traces collected by Peru’s DCT application, we proposed a lightweight Spatial-Neighbourhood Fusion (SPN) step and demonstrated its effectiveness across three forecasting backbones. SPN consistently reduces error up to **9.85%**—with minimal overhead. Notably, the convolutional *K-U-Net* surpasses *PatchTST* in accuracy while being roughly **2× faster** in training and inference, making it well-suited for real-time deployment. These findings underscore the value of local spatial context and show that simple, model-agnostic fusion strategies can enhance mobility forecasting in public-health settings.

Ethics Statement

This study uses anonymized mobility data collected through Peru’s national Digital Contact Tracing (DCT) application, developed under CONCYTEC Project No. 70744. All personal identifiers were irreversibly hashed using SHA-256, and data collection was based on informed user consent. Participation was voluntary, and only aggregated, non-identifiable data were accessed by researchers. The study complies with all applicable data protection regulations and ethical standards.

7 Appendix

Plot samples The figure below shows the prediction results for a sample input length of 48, 72, 96 and 120.

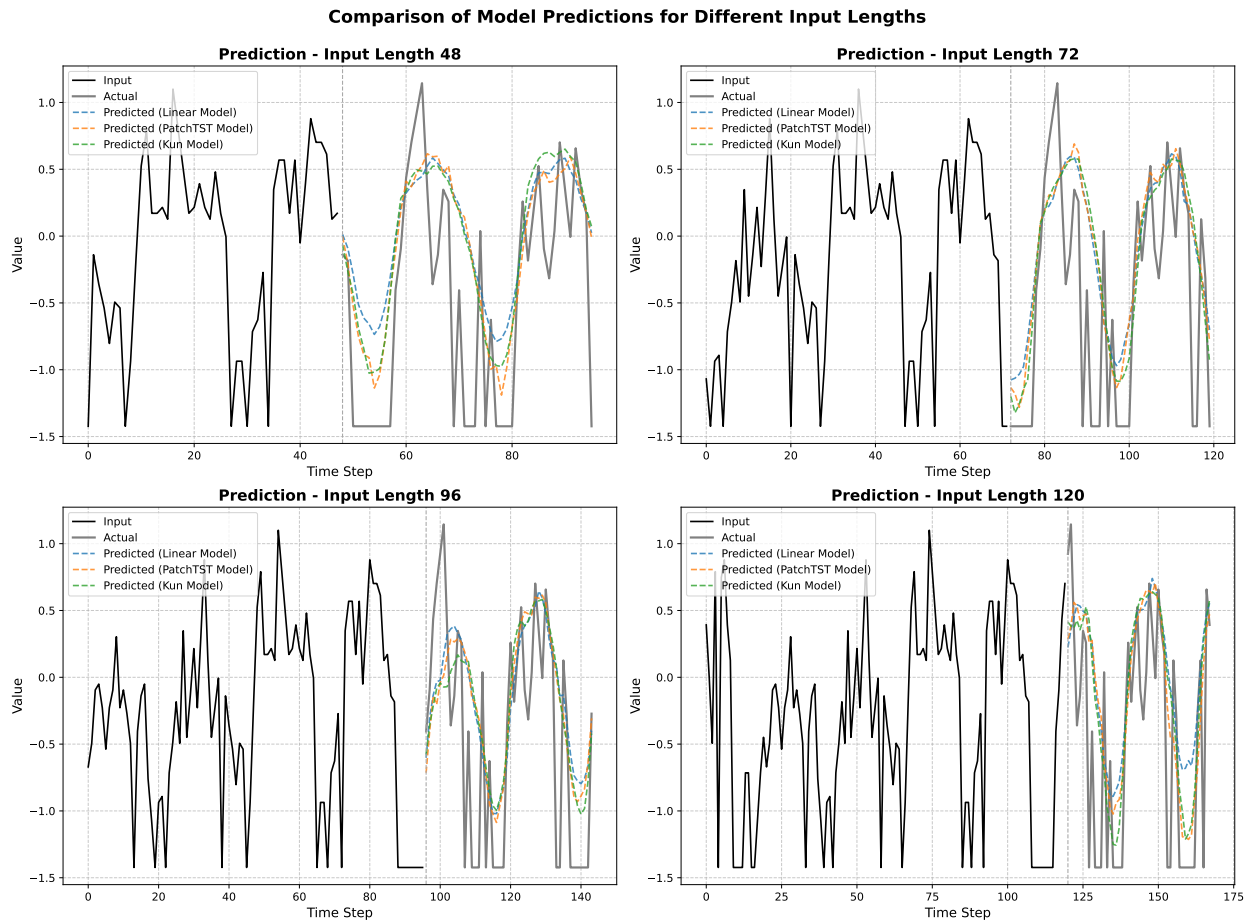


Figure 3: Comparison of predicted sequences across models.

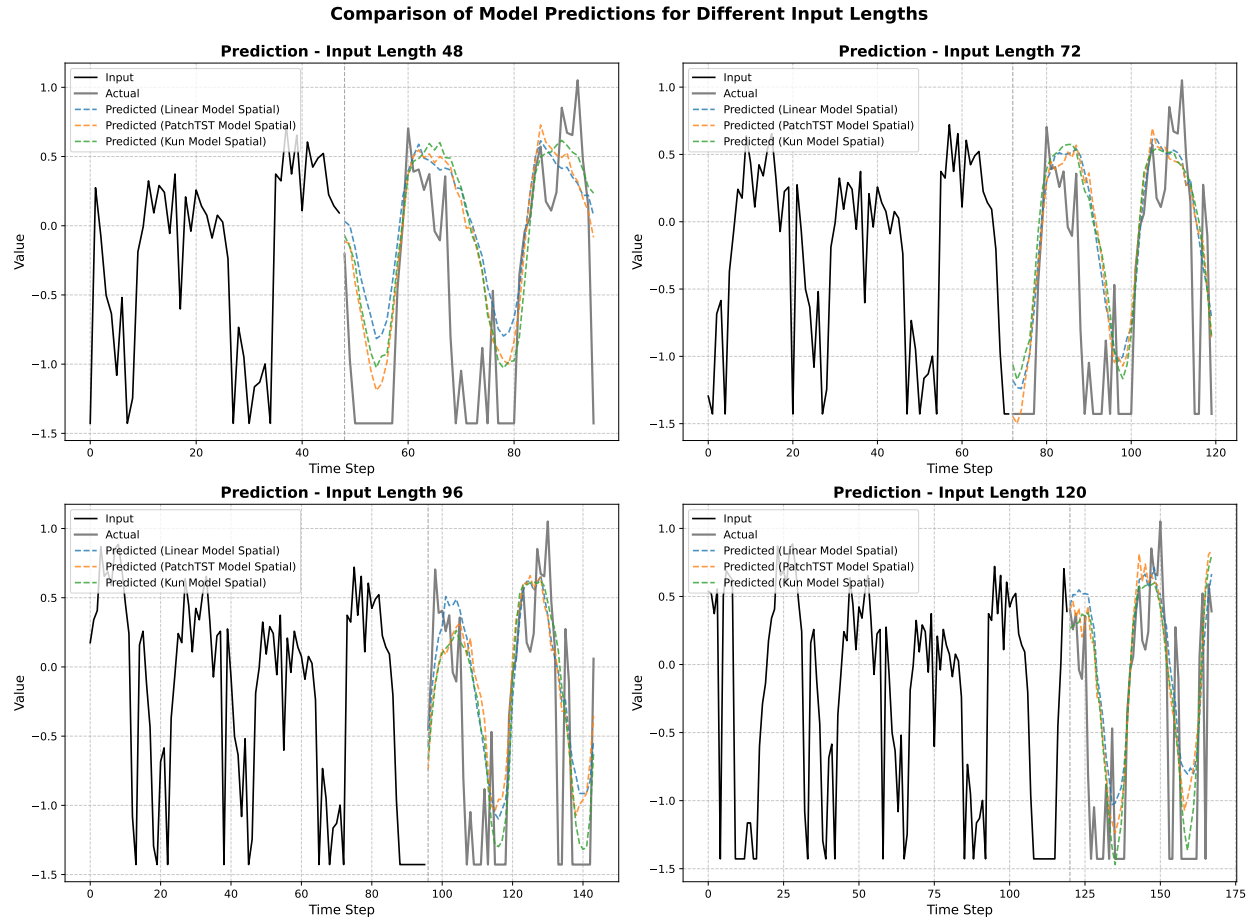


Figure 4: Comparison of predicted sequences with SPN features across models.

References

- [1] Nuria Oliver, Bruno Lepri, Harald Sterly, Renaud Lambiotte, Sébastien Deletaille, Marco De Nadai, Emmanuel Letouzé, Albert Ali Salah, Richard Benjamins, Ciro Cattuto, et al. Mobile phone data for informing public health actions across the covid-19 pandemic life cycle, 2020.
- [2] Cornelia Ilin, Sébastien Annan-Phan, Xiao Hui Tai, Shikhar Mehra, Solomon Hsiang, and Joshua E Blumenstock. Public mobility data enables covid-19 forecasting and management at local and global scales. *Scientific reports*, 11(1):13531, 2021.
- [3] Sacha Alanoca, Nicolas Guetta-Jeanrenaud, Isabela Ferrari, Nyasha Weinberg, R Buse Cetin, and Nicolas Mialhe. Digital contact tracing against covid-19: a governance framework to build trust. *International Data Privacy Law*, 11(1):3–17, 2021.
- [4] Inc. Uber Technologies. H3: A hexagonal hierarchical spatial index. <https://h3geo.org>, 2024. Accessed: 2025-05-02.
- [5] Pranay Pherwani, Nicholas Hass, and Anna Yanchenko. Spatiotemporal modeling and forecasting at scale with dynamic generalized linear models. In *Proceedings of the 1st ACM SIGSPATIAL International Workshop on Geospatial Anomaly Detection*, pages 16–27, 2024.
- [6] Yihong Ma, Patrick Gerard, Yijun Tian, Zhichun Guo, and Nitesh V Chawla. Hierarchical spatio-temporal graph neural networks for pandemic forecasting. In *Proceedings of the 31st ACM International Conference on Information & Knowledge Management*, pages 1481–1490, 2022.
- [7] Yuqi Nie, Nam H. Nguyen, Phanwadee Sinthong, and Jayant Kalagnanam. A time series is worth 64 words: Long-term forecasting with transformers. *International Conference on Learning Representations*, 2023.
- [8] Zhenyu Han, Fengli Xu, Yong Li, Tao Jiang, and James Evans. Model predicted human mobility explains covid-19 transmission in urban space without behavioral data. *Scientific Reports*, 15(1):6365, 2025.
- [9] Matteo Serafino, Higor S Monteiro, Shaojun Luo, Saulo DS Reis, Carles Igual, Antonio S Lima Neto, Matías Travizano, José S Andrade Jr, and Hernán A Makse. Digital contact tracing and network theory to stop the spread of covid-19 using big-data on human mobility geolocalization. *PLOS Computational Biology*, 18(4):e1009865, 2022.
- [10] Guangyin Jin, Yuxuan Liang, Yuchen Fang, Zezhi Shao, Jincan Huang, Junbo Zhang, and Yu Zheng. Spatio-temporal graph neural networks for predictive learning in urban computing: A survey. *IEEE Transactions on Knowledge and Data Engineering*, 36(10):5388–5408, 2023.
- [11] Ailing Zeng, Muxi Chen, Lei Zhang, and Qiang Xu. Are transformers effective for time series forecasting? In *Proceedings of the AAAI Conference on Artificial Intelligence*, 2023.
- [12] Eleonora Arnone, Laura M Sangalli, and Andrea Vicini. Smoothing spatio-temporal data with complex missing data patterns. *Statistical Modelling*, 23(4):327–356, 2023.
- [13] Zhengyan Cui, Junjun Zhang, Giseop Noh, and Hyun Jun Park. Adstgcn: A dynamic adaptive deeper spatio-temporal graph convolutional network for multi-step traffic forecasting. *Sensors*, 23(15):6950, 2023.
- [14] Christopher D Elvidge, Kimberly Baugh, Mikhail Zhizhin, Feng Chi Hsu, and Tilottama Ghosh. Viirs night-time lights. *International journal of remote sensing*, 38(21):5860–5879, 2017.
- [15] Christopher Small. Spatiotemporal characterization of viirs night light. *Frontiers in Remote Sensing*, 2:775399, 2021.
- [16] Yuping Wang and Zehao Shen. Comparing luojia 1-01 and viirs nighttime light data in detecting urban spatial structure using a threshold-based kernel density estimation. *Remote Sensing*, 13(8):1574, 2021.
- [17] Changyong Cao, Bin Zhang, Frank Xia, and Yan Bai. Exploring viirs night light long-term time series with cnn/si for urban change detection and aerosol monitoring. *Remote Sensing*, 14(13):3126, 2022.
- [18] Jiang You, René Natowicz, Arben Cela, Jacob Ouanounou, and Patrick Siarry. Kernel-u-net: Symmetric and hierarchical architecture for multivariate time series forecasting. <https://arxiv.org/abs/2401.01479>, 2024.